Degradation and State of Health Prediction of a Battery used in a Microgrid in Real-time

Laxman Timilsina[1*], Ali Moghassemi[1], Elutunji Buraimoh[1], SM Imrat Rahman[1], Asif Ahmed Khan[1], Grace Muriithi[2], Gokhan Ozkan[1,3], Behnaz Papari[1,2], Christopher S. Edrington[1]
E-mails: {ltimils*, amoghas, eburaim, smimrar, asifahm, gmuriit, gokhano, bpapari, cedring}@clemson.edu
[1]*Holcombe Department of Electrical and Computer Engineering, Clemson University, Clemson 29634, SC, USA*
[2]*Department of Automotive Engineering, Clemson University, Greenville 29607, SC, USA*
[3]*Dominion Energy Innovation Center, Clemson University, North Charleston 29405, SC, USA*

2024 IEEE Sixth International Conference on DC Microgrids (ICDCM) | 979-8-3503-6363-0/24/$31.00 ©2024 IEEE | DOI: 10.1109/ICDCM60322.2024.10665285

***Abstract*—Battery degradation is a complex physicochemical phenomenon intricately influenced by operational parameters and environmental factors. This paper delves into the degradation of lithium-ion batteries within microgrid systems, utilizing historical aging data from the University of Wisconsin-Madison to train a degradation model employing neural networks. The dataset is transformed to align with the battery pack rating pertinent to this investigation. The study identifies and examines several contributing factors to battery degradation, with a specific focus on temperature, charging current, discharging current, and depth of discharge. Emphasizing the significance of these parameters, particularly the latter three, the research endeavors to predict battery degradation in diverse operational conditions within a Microgrid system. This study modeled a Microgrid configuration capable of operating in islanded and grid-connected mode featuring solar PV, wind, a diesel generator, and a battery. Real-time simulations of different operational scenarios are conducted using the digital real-time simulator. Additionally, the battery's operational status is sent to a controller to predict its degradation and state of health. The controller used here is a Raspberry Pi, and communication is facilitated through UDP protocol.**

***Index Terms*—microgrid, lithium-ion battery, degradation, forecasting**

I. Introduction

In recent years, batteries have emerged as indispensable components within Microgrid systems. Battery energy storage systems play a pivotal role in enhancing the integration of intermittent renewable energy sources such as solar PV and wind into the grid. Their adaptability in storing surplus energy during periods of high generation and releasing it during peak demand hours has significantly contributed to smoothing out the variability inherent in renewable energy output, thereby enhancing its reliability and predictability [1], [2].

Batteries serve as a reliable backup power source for critical loads during grid outages, ensuring uninterrupted operation of essential services. Additionally, they contribute to grid stability by effectively managing supply and demand fluctuations. Their rapid response capability enables them to adjust to changes in load or generation, thereby maintaining a stable frequency and voltage within the grid. Also, batteries play a significant role in mitigating peak demand by supplying stored energy during periods of heightened electricity consumption. This alleviates strain on the main grid infrastructure, leading to potential reductions in electricity costs and improvements in overall grid reliability [3].

Therefore, batteries have been used in a Microgrid system to minimize the instability arising from the intermittent nature of renewable energy sources. This integration enhances control, predictability, and stability of power output [4], [5]. Study [6], [7] considers incorporating batteries at various renewable energy penetration levels, reducing unsatisfied demand, halving the number of sources, and lowering CO_2 emission intensity. The characteristics of lithium-ion batteries, including fast response, low self-discharge, and long cycle life, contribute to primary frequency and voltage regulation and peak load reduction [8].

As the demand for integrating distributed renewable energy sources and the pressure from electric vehicle (EV) fast charging on the utility grid continues to rise, the DC microgrid is recognized as a viable solution and a crucial technology for enhancing photovoltaics (PV) penetration, facilitating EV adoption, and improving energy transmission efficiency [8]. However, a significant challenge in promoting DC microgrids stems from the substantial economic costs associated with their construction and operation. Among various expenses, the cost of the battery within the microgrid system holds significance, and furthermore, its operational lifespan is shorter compared to other components in the microgrid. Additionally, the battery's lifecycle is substantially influenced by the operating conditions [9]. Therefore, precise monitoring of the battery condition is essential, and appropriate actions can be taken based on its degradation rate. This can involve employing various strategies, such as adjusting energy management [10].

The Microgrid system illustrated in Fig. 1 is used as the experimental platform in this study. This system is constructed in a Typhoon schematic editor and is simulated in real-time using the Typhoon HIL 606 simulator. While the Microgrid has the capability to connect to the main grid via a grid-forming converter and a transformer, this study concentrates on its operation in islanded mode only, with particular emphasis on observing the behavior of the battery under various conditions and its aging process.

The power generation sources in this system comprise Solar

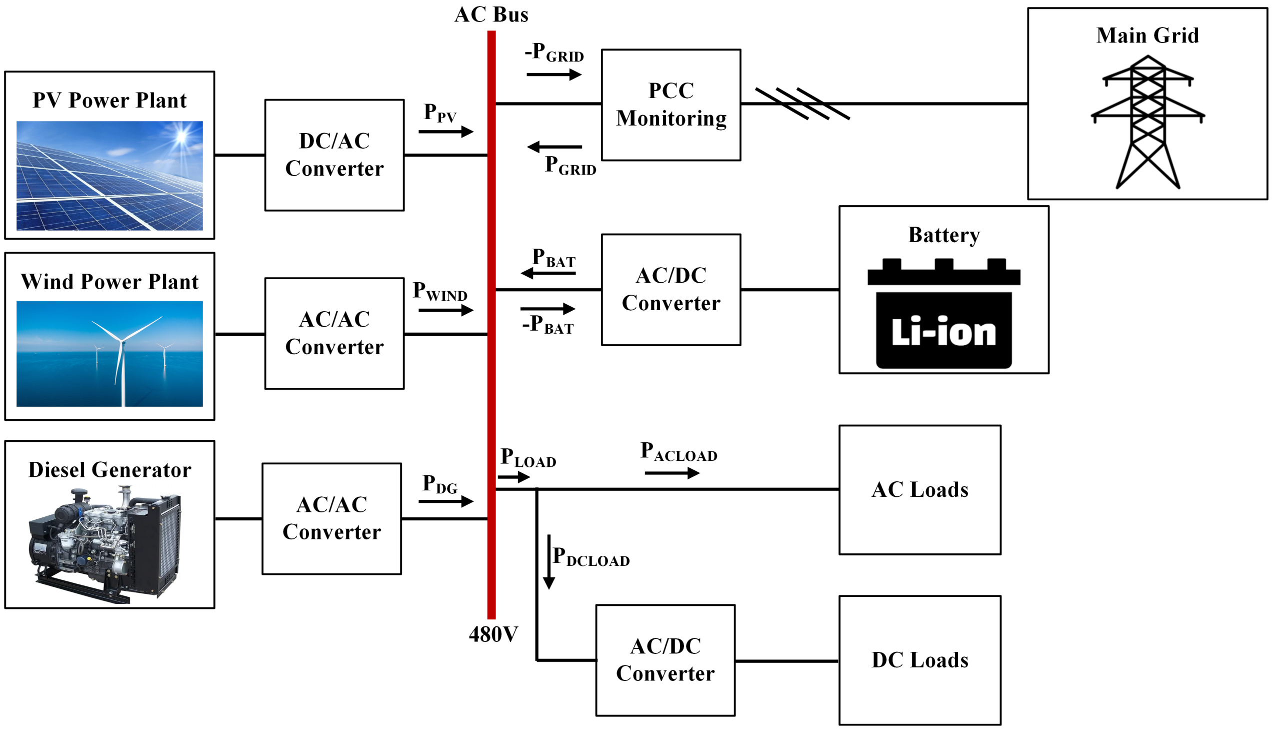

Fig. 1: Schematic diagram of the Microgrid system considered in this study.

PV, a Wind power plant, a diesel generator, and a lithium-ion battery pack. Additionally, both DC and AC loads with constant and variable loads are incorporated into the system. These power sources are controlled and operated independently at different time intervals, allowing for the examination of diverse operational scenarios to predict battery degradation.

A. Statement of Contribution

The cost associated with the battery in a microgrid constitutes a significant portion of the overall expenditure. If the battery degradation rate is high, it could render the system economically unviable over time, especially if frequent replacements are necessary due to accelerated degradation. Consequently, continuous monitoring of battery degradation is imperative, and proactive control measures through microgrid energy management (EM) must be implemented to extend the battery's operational lifespan.

Addressing the challenge of accurately predicting battery aging, this paper proposes a novel modeling technique tailored to forecast the degradation of batteries deployed within microgrid systems. Moreover, to validate the proposed approach, the study integrates a microgrid system into a real-time simulator, specifically Typhoon HIL 606, and employs a data-driven technique to achieve battery degradation modeling. This modeling is then implemented in a Raspberry Pi, serving as a controller within the microgrid setup.

The real-time prediction of battery aging facilitated by this approach holds promise for future research endeavors, particularly in utilizing it as a control metric within microgrid energy management systems. By leveraging this predictive capability, future studies can aim to devise strategies aimed at mitigating battery aging, thereby prolonging the operational lifespan of batteries deployed in microgrid systems.

The remaining paper is segmented as follows: Section II explains the Microgrid system considered in this study. Section III explains in detail the modeling of the battery degradation prediction in detail. The different operating scenario for the Microgrid system and the results is explained in detail in Section IV. Finally, Section V provides the paper's conclusion and suggests future research directions.

II. Microgrid System

The structure of a generic Microgrid, as depicted in Fig. 1 and considered in this study, encompasses key renewable energy sources such as wind and solar. These sources are seamlessly integrated into the system through power converters. In addition to these primary energy sources, the MG incorporates essential components such as a Battery Energy Storage System (BESS), a diesel generator (DG), and various loads. All these sources and loads are interconnected to a 480V AC bus, and the microgrid has the capability to connect to the main grid, as illustrated in the figure. While AC loads are directly supplied, DC loads receive power through a power electronic converter (rectifier).

In addition to the generators, storage elements, and other necessary equipment for operation, the MG features a centralized control system. In this study, the microgrid operates exclusively in islanded mode, with the central controller making decisions regarding resource handling. To maintain simplicity in the central control system, the microgrid operates based on power supply and demand constraints. The power demanded by the loads is met and supplied by the available sources. Detailed explanations regarding the activation and deactivation of different sources for battery degradation analysis will be provided in Section IV.

The microgrid system comprises various components, each with specific ratings tailored to meet operational requirements. The battery operates at a nominal terminal voltage of 1000V and has a storage capacity of 500Ah. A converter is utilized to adjust the terminal output voltage to 480V AC for connection to the AC bus. The maximum power generating capacity of the solar PV panels is 250 kW, with a PV inverter load ratio of 1.2.

Similarly, the wind power plant has a capacity of 500 kW, operating at a nominal wind speed of 13 m/s. The diesel generator is capable of supplying a nominal active power of 800 kW, with a nominal speed of 1800 rpm, providing backup power during low renewable energy generation or emergencies.

Moreover, the microgrid accommodates three types of loads: interruptible, variable, and constant. The variable load is rated at 450 kW with a power factor of 0.85, while the constant impedance load and interruptible load are rated at 700 kVA and 480 VA, respectively, both with a power factor of 0.95.

For the battery, as explained earlier, the nominal voltage is 1000V with a 500Ah capacity. To simulate battery aging, a battery cell tested at the laboratory of the University of Wisconsin is utilized. To achieve a battery pack with a capacity of 1000V and 500Ah, derived from 2.9Ah cells with a nominal voltage of 3.7V, a combination of series and parallel connections is essential. Initially, the calculation entails determining the number of cells required in series to achieve the desired voltage:

$$\text{Number of cells in series} = \frac{\text{Desired voltage}}{\text{Nominal voltage per cell}} \approx 271$$

Subsequently, to meet the targeted capacity of 500Ah, cells must be connected in parallel. Given each cell's capacity of 2.9Ah:

$$\text{Number of cells in parallel} = \frac{\text{Desired capacity}}{\text{Capacity per cell}} \approx 173$$

Consequently, approximately 271 cells are connected in series, and 173 sets of these series-connected cells are connected in parallel, which is necessary to realize a battery pack with a capacity of 1000V and 500Ah.

III. Battery Degradation Modeling and Prediction

Several investigations have employed analytical and data-driven methodologies to forecast future events, such as the aging of batteries. Studies by [11] and [12] utilized the Markov chain method for predicting battery aging. However, this approach may become computationally burdensome with large datasets, and capturing the non-linear relationships using Markov chains can be challenging. Additionally, the computation of an additional variable, the "transition matrix," is required in this process. Consequently, data-driven methods like neural networks can offer advantages over the Markov chain method for such purposes, as they are not subject to these issues.

Studies [13] and [14] have used data-driven methods to predict battery degradation patterns. In study [13], a convolutional neural network was employed to predict battery degradation paths. Sufficient historical aging data is essential for effectively training these neural networks. Following this, this paper also employs data-driven techniques, specifically neural networks, to forecast the aging patterns of batteries within a microgrid system. The study utilizes a dataset acquired from the University of Wisconsin-Madison, which pertains to testing a newly acquired 2.9Ah Panasonic 18650PF cell. The testing was conducted within an 8 cubic-foot thermal chamber using a 25 amp, 18-volt digatron firing circuits universal battery tester channel. This dataset includes a variety of aging tests conducted at five different temperatures: 25°C, 10°C, 0°C, −10°C, and −20°C [15]. Each temperature setting consists of ten distinct aging datasets, all of which are utilized in the training, testing, and validation procedures of the neural networks.

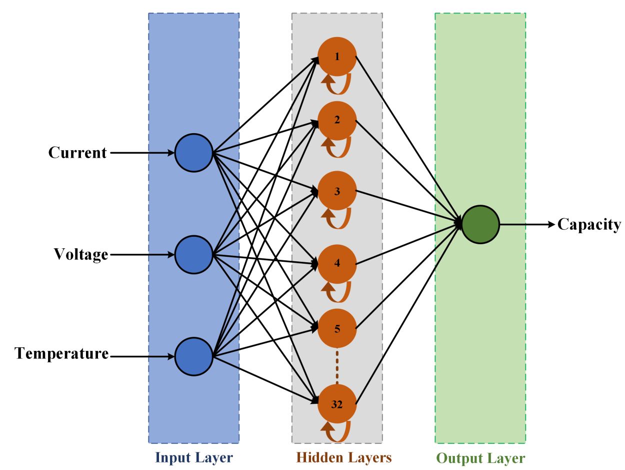

Fig. 2: Architecture of the neural network considered.

Similar to study [13], the predictive model in this study adopts a three-layer neural network architecture consisting of an input layer, a hidden layer, and an output layer, specifically designed to forecast battery capacity loss, as shown in Fig. 2. Prior to model input, the data undergo pre-processing, and essential features—voltage, current, temperature, and capacity—are extracted. The neural network's input layer accommodates three inputs: current, voltage, and temperature, while the output layer predicts battery capacity.

Three neural networks are modeled to predict capacity loss: feedforward neural network (FNN), recurrent neural network (RNN) using LSTM cells, and deep neural network (DNN). For all the networks, there are three layers comprising three neurons in the input layer, one neuron in the output layer,

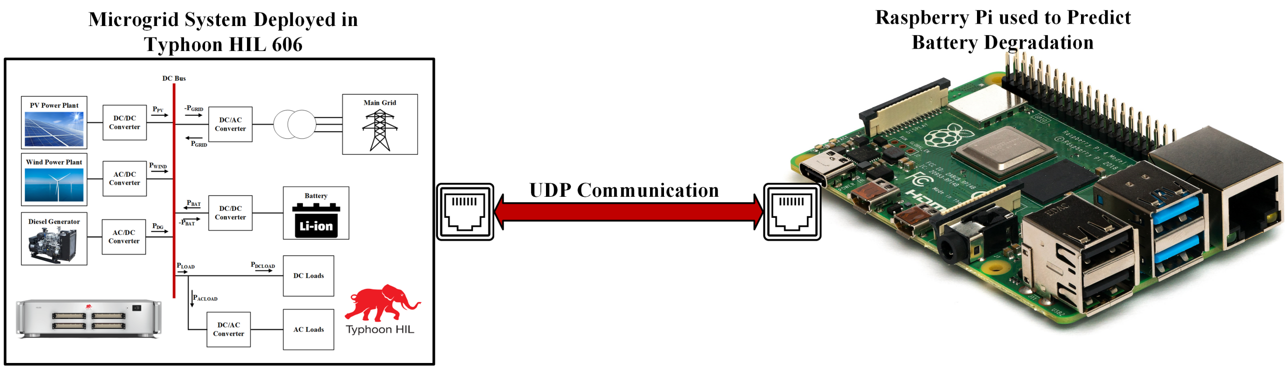

Fig. 3: Real-time implementation of the proposed system.

and one hidden layer with 32 neurons for FNN and RNN. In contrast, for DNN, there are two hidden layers with 32 and 16 neurons on these layers. The dataset is segregated into distinct subsets for training, testing, and validation purposes.

To assess the models more comprehensively, metrics such as mean absolute error (MAE), mean square error (MSE), and R-squared (R2) are used. Table I presents a comparison of the fitting of these three techniques. It is evident from the table that the RNN (LSTM) network outperforms the other two networks, exhibiting lower MSE, MAE values and higher R2 values for the training/testing dataset. Additionally, the DNN model demonstrates the second-best fitting performance, while the FNN lags behind the other two models in terms of accuracy.

TABLE I: Comparison of Fitting of Different Neural Networks

Parameters	**FNN**	**RNN-LSTM**	**DNN**
MAE	0.0789	0.0687	0.0697
MSE	0.0129	0.0091	0.0096
R-Square	0.9743	0.984	0.9808

Therefore, the LSTM neural network is employed to construct the degradation model. Fig. 4 illustrates the comparison of the predicted degradation path generated by this model for an unused dataset with the actual degradation path, which was not part of the training, testing, or validation processes. The corresponding metrics for this prediction are an MAE of 0.0728, an MSE of 0.0088, and an R-square value of 0.9860.

The capacity loss in watt-hours is calculated through this neural network. Subsequently, to ascertain the battery's remaining useful life, it can be subtracted from the initial capacity using the formula provided in (1), yielding the battery's remaining life or state of health (SOH).

$$\text{Capacity Loss } (\%) = \frac{\text{Capacity Loss}}{\text{Initial Capacity}} \times 100\% \tag{1a}$$

$$\text{SOH} = \frac{\text{Initial Capacity} - \text{Capacity Loss}}{\text{Initial Capacity}} \times 100\% \tag{1b}$$

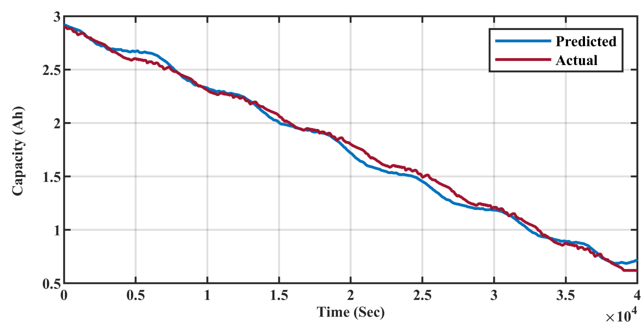

Fig. 4: Comparison of prediction of neural network output with the actual pattern.

IV. Real Time Implementation and Results

As previously elucidated, the simulation operates in real-time utilizing a Microgrid system, illustrated in Fig. 1, deployed within a Typhoon HIL 606 digital real-time simulator. This deployment on a real-time simulator serves further to affirm the efficacy and resilience of the developed system. As expounded upon in Section III, the LSTM neural network exhibits superior performance compared to alternative networks; thus, it is employed for predicting battery degradation. To facilitate degradation pattern prediction, the Raspberry Pi 4 Model B is utilized as shown in Fig. 3. The requisite code for degradation prediction, along with the LSTM model, is deployed within the Pi.

As delineated, the input data encompasses three features: voltage, current, and temperature. To facilitate comparison across networks, all three networks employ 32 hidden layers (with the first hidden layer of the DNN network), utilizing the Rectified Linear Unit (ReLU) function as the activation function. ReLU is chosen for its ability to capture intricate non-linear relationships, thereby enhancing predictive performance. The output layer comprises a single neuron tasked with predicting battery capacity loss, devoid of any specified activation function to ensure raw output values directly represent the predicted continuous output.

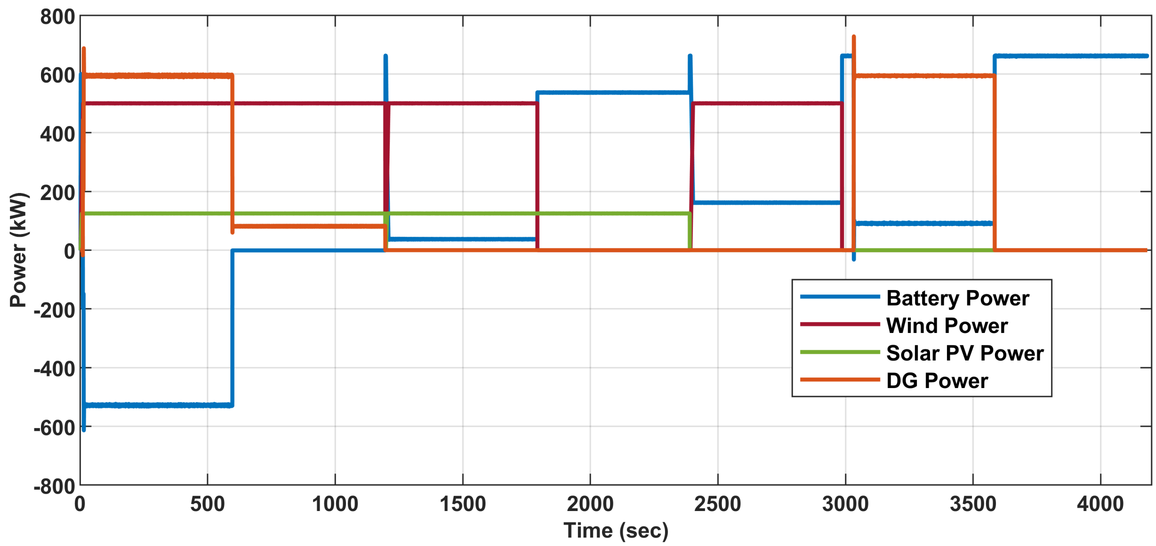

Fig. 5: Power supplied by different sources in the Microgrid.

The models are compiled utilizing the mean squared error (MSE) as the loss function and the Adam optimizer. The forward function executes the forward pass of the model, taking input data, passing it through the hidden layer to obtain the hidden state, and then applying the fully connected layer to generate the output. PyTorch library is utilized for training and development, leveraging training data and corresponding target values and training is conducted over 100 epochs.

Now, the neural network requires inputs to be transmitted from the Typhoon to the Raspberry Pi. The UDP protocol is utilized to facilitate this communication. The data forwarded from the Typhoon encompass the battery pack's voltage, the current either supplied to or drawn from the battery, and the temperature of the battery pack. Utilizing these inputs, the Raspberry Pi computes the battery's capacity loss. Subsequently, the computed capacity loss, along with the battery's remaining capacity, is transmitted back to the Typhoon for visualization purposes.

Since this study is primarily concerned with predicting battery aging, the simulation focuses on the Microgrid's operation involving the battery. To this end, the Microgrid is analyzed in islanded mode. The total simulation duration for this investigation is set at 70 minutes and divided into seven distinct operational phases, each with 10 minutes, as highlighted in Table II. Prior to commencing the simulation, the battery's state of charge (SoC) is initialized to 50%. The power supplied by each source during these different operational phases is shown in Fig. 5. Furthermore, for the sake of simplicity in the simulation, a constant impedance load rated at 700 kVA with power factor of 0.95 is continuously active. In this study, the variable load remains inactive. Consequently, with a lagging power factor of 0.95, the load demands 665 kW of power.

Throughout various operational scenarios, the battery undergoes charging when the available power exceeds the load demand. Emphasizing cost efficiency, preference is accorded to renewable sources over DG. Conversely, when load demand surpasses available power, the battery provides supplementary power. Consequently, during the charging phases, the battery exhibits a negative current, while during the power supply phases, the battery's current is positive, as depicted in Fig. 6. Furthermore, the terminal voltage of the battery fluctuates in response to its charging and discharging cycles, a phenomenon elucidated in Fig. 7.

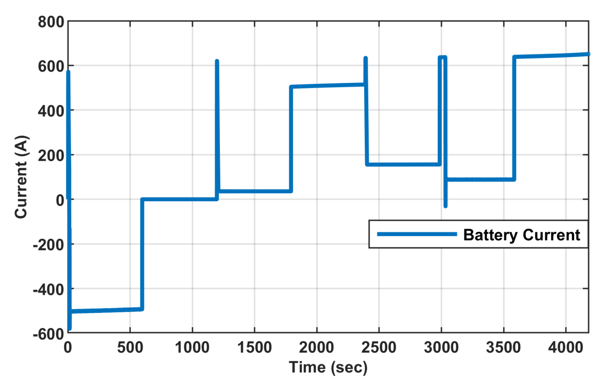

Fig. 6: Current supplied by the battery.

In the initial scenario, all power-generating sources, comprising wind, solar PV, DG, and the battery, are simultaneously activated for a duration of 10 minutes. Since the load demand is lower than the total power generation, surplus power is utilized to charge the battery, as evidenced by the negative power for the battery in Fig. 5. This observation is further corroborated by Fig. 6, illustrating negative current, and Fig. 7, depicting a rise in the terminal voltage of the battery. Moreover, Fig. 8 showcases an increase in the SoC of the battery.

TABLE II: Different Operating Scenarios of the Microgrid System

Time	**10 mins**	**10 mins**	**10 mins**	**10 mins**	**10 mins**	**10 mins**	**10 mins**
Sources Off	None	Battery Off	DG Off	DG and Wind Off	DG and PV Off	Wind and PV Off	DG, Wind, and PV Off
Sources On	All sources On	DG, Wind, and PV On	Battery, Wind, and PV On	Battery and PV On	Battery and Wind On	Battery and DG On	Battery On

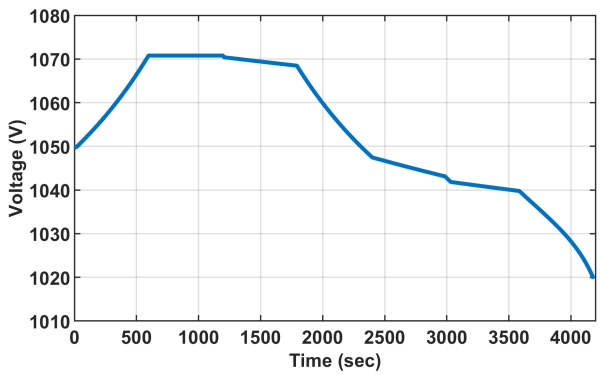

Fig. 7: Terminal voltage of the battery.

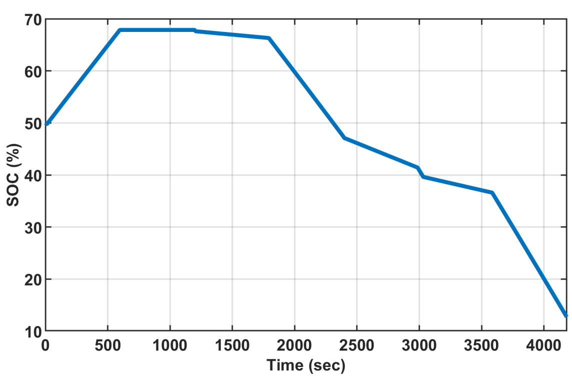

Fig. 8: SoC of the battery.

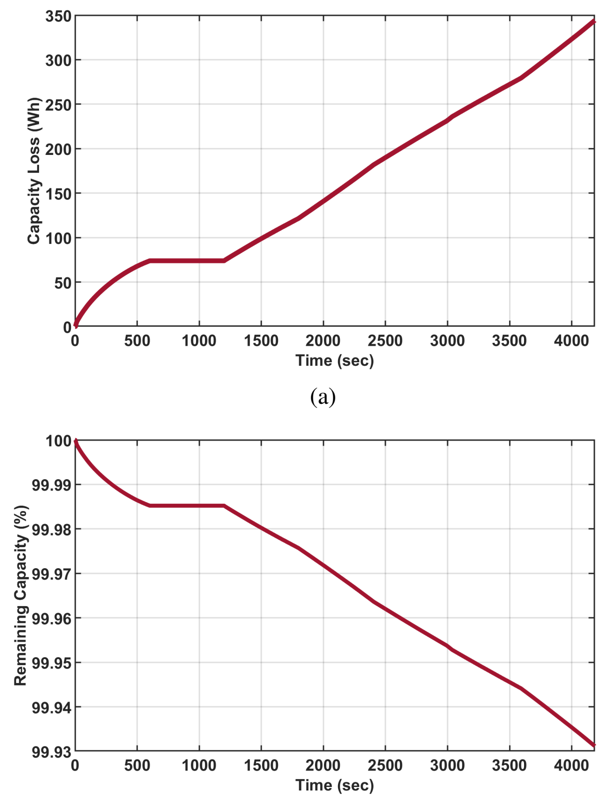

(a)

(b)

Fig. 9: Battery (a) Capacity loss and (b) Degradation pattern

Transitioning to the second scenario, the battery is deactivated, with only wind, solar PV, and DG serving as the available power sources. Consequently, with the battery out of operation, the current supplied by it is zero, as evidenced in Fig. 6. Additionally, both the voltage of the battery pack and the SoC remain constant, as depicted in Figs. 7 and 8, respectively.

Moving to the third scenario, DG is disabled, leaving the battery, wind, and solar PV as the primary power sources. However, the combined power generated by the wind and solar PV is insufficient to meet the load demand. Consequently, the battery supplements the power supply by providing approximately 35 kW of power. This augmentation is evident from the positive values of power and current illustrated in Figs. 5 and 6, respectively. Furthermore, there is a discernible decline in both the voltage and SoC of the battery, as observed in Figs. 7 and 8, respectively.

In the fourth operational scenario, wind and DG are deactivated, with the battery and PV serving the load. As the load demand exceeds the power generated by solar alone, the battery supplements the power supply, as evidenced by the positive power of the battery in Fig. 5. Additionally, Fig. 6 depicts positive current, and Fig. 7 indicates a decline in the terminal voltage, confirming the battery's power supply. Consequently, the SoC of the battery decreases, as depicted in Fig. 8.

In the fifth scenario, wind and PV sources are disabled, leaving the battery and DG to fulfill the load requirements. Similarly, in the sixth scenario, both DG and PV sources are deactivated, and the load is sustained by the battery and wind turbine. As the load demand exceeds the power generated by the sources in both scenarios, the battery contributes to the power supply. This contribution is evident from the positive power of the battery in Fig. 5, the positive current in Fig. 6, and the declining terminal voltage in Fig. 7. Consequently, there is a corresponding decrease in the SoC of the battery, as demonstrated in Fig. 8.

Finally, in the seventh scenario, all power sources, including wind, DG, and PV, are deactivated, leaving only the battery to meet the load demand. In this case, the battery bears the entire load, resulting in the highest amount of discharging current, as depicted in Fig. 6. Additionally, the terminal voltage and the SoC of the battery decrease rapidly, as illustrated in Figs. 7 and 8, respectively.

The essential inputs required by the neural network to forecast the battery's degradation trajectory are depicted in Fig. 6 and Fig. 7, respectively. Additionally, the battery temperature, presumed to operate at ambient conditions, is transmitted from the Typhoon to the Raspberry Pi via UDP communication. Leveraging these data, the controller calculates the battery's capacity loss, measured in watt-hours. Subsequently, to determine the battery's remaining useful life, the calculated capacity loss is subtracted from the initial capacity using the formula provided in (1). This computation yields the battery's remaining life or SOH. Finally, upon computing these two metrics—capacity loss and remaining battery capacity—they are relayed back to the Typhoon for visualization via UDP communication. The results for the capacity loss and the remaining battery capacity are displayed in Fig. 9a and Fig. 9b, respectively.

V. Conclusion and Future Works

The complex nature of battery degradation necessitates precise estimation to ensure the system's dependable operation and timely maintenance, thereby enhancing overall reliability. This study proposed a real-time approach tailored for predicting battery degradation and determining its remaining capacity, often referred to as the SOH, within the dynamic setting of a Microgrid. Leveraging the capabilities of a Recurrent Neural Network (RNN), this study constructed a degradation model specifically designed to capture the complex interplay of factors influencing battery health over time.

To enable real-time monitoring and analysis, the degradation model is implemented on a Raspberry Pi, establishing seamless communication via UDP protocol with the Microgrid system simulated on Typhoon, a digital real-time simulator. This integration facilitates continuous data exchange and enables rapid assessment of battery performance under varying operational conditions. The evaluation of battery aging is conducted under seven distinct scenarios, each representing different operating scenarios of the Microgrid where various power sources are selectively activated or deactivated. Subjecting the battery to these diverse operating conditions, the impact on the degradation of the battery and, subsequently, SOH is calculated.

Determining the battery's degradation rate serves as a key control metric for energy management, enabling proactive adjustments to optimize overall system performance and extend its operational lifespan. This aspect represents a prospective avenue for future exploration within the scope of this study.

Acknowledgment

The authors would like to acknowledge the Warren H. Owen Distinguished Professorship Endowment for its support of the research effort.

References

[1] I. Alsaidan, A. Khodaei, and W. Gao, "A comprehensive battery energy storage optimal sizing model for microgrid applications," *IEEE Transactions on Power Systems*, vol. 33(4), 2017.

[2] A. Arsalan, J. Ahmad, M. Tahir and S. K. Mazumder, "Distributed Control and Power Management of Islanded DC Nanogrids with Applications to Rural Electrification," 2020 IEEE Energy Conversion Congress and Exposition (ECCE), Detroit, MI, USA, 2020, pp. 4662-4667, doi: 10.1109/ECCE44975.2020.9236352.

[3] Q. Fu, A. Hamidi, A. Nasiri, V. Bhavaraju, SB. Krstic, P. Theisen, "The Role of Energy Storage in a Microgrid Concept: Examining the opportunities and promise of microgrids," *IEEE Electrification Magazine*, vol. 1(2), 2013.

[4] Sarwar, Sohail, et al. "Enhanced energy balancing and optimal load curtailment strategy for DC microgrid integration in hybrid AC/DC distribution networks." IET Smart Grid (2024).

[5] N. Shamarova, K. Suslov, P. Ilyushin, and I. Shushpanov, "Review of Battery Energy Storage Systems Modeling in Microgrids with Renewables Considering Battery Degradation," Energies 15, no. 19 (2022): 6967. ," *Energies*, vol. 15(19), 2022.

[6] MS. Zantye, A. Gandhi, Y. Wang, SP. Vudata, D. Bhattacharyya, and MF. Hasan, "Optimal design and integration of decentralized electrochemical energy storage with renewables and fossil plants," *Energy & Environmental Science*, vol. 15(10), 2022.

[7] Arsalan, Ali, et al. "A Resilient Distributed Control and Energy Management Approach for DERs and EVs with Application to EV Charging Stations." IFAC-PapersOnLine 56.2 (2023): 2115-2120.

[8] S. Wang, D. Guo, X. Han, L. Lu, K. Sun, W. Li, DU. Sauer, and M. Ouyang, "Impact of battery degradation models on energy management of a grid-connected DC microgrid," *Energy*, vol. 207, 2020.

[9] L. Timilsina, P.R. Badr, P. H. Hoang, G. Ozkan, B. Papari, and C. S. Edrington, "Battery degradation in electric and hybrid electric vehicles: A survey study," *IEEE Access*, vol. 11, pp. 42431-42462, 2023.

[10] S. Ouédraogo, GA. Faggianelli, G. Pigelet, G. Notton, and JL. Duchaud, "Performances of energy management strategies for a Photovoltaic/Battery microgrid considering battery degradation," *Solar Energy*, vol. 230, 2021.

[11] L. Timilsina, P. H. Hoang, A. Moghassemmi, P.K. Chamarthi, G. Ozkan, B. Papari, and C. S. Edrington, "A Real-Time Prognostic Based Control Framework for Hybrid Electric Vehicles," *IEEE Access*, vol. 11, pp. 127589 - 127607, 2023.

[12] P. H. Hoang, G. Ozkan, P. R. Badr, L. Timilsina, B. Papari, and C. S. Edrington, "Integrating degradation forecasting into distribution grids' advanced distribution management systems," *International Journal of Electrical Power & Energy Systems*, vol. 150, pp. 109071, 2023.

[13] N. Costa, L. Sánchez, D. Anseán, and M. Dubarry, "Li-ion battery degradation modes diagnosis via Convolutional Neural Networks," *Journal of Energy Storage*, vol. 55, 2022.

[14] L. Timilsina, P. H. Hoang, A. Arsalan, G. Ozkan, B. Papari, and C. S. Edrington, "Degradation Abatement In Hybrid Electric Vehicles Using Data-driven Technique," *Transportation Research Procedia*, vol. 70, pp. 52-60, 2023.

[15] P. Kollmeyer, "Panasonic 18650pf li-ion battery data. Mendeley Data," vol. 1, 2018.